DOI 10.1016/j.scitotenv.2017.04.191

Adsorption process of fluoride from drinking water with magnetic core-shell Ce-Ti@Fe_3O_4 and Ce-Ti oxide nanoparticles

Ahmad Abo Markeb, Amanda Alonso*, Antoni Sánchez, Xavier Font

Department of Chemical, Biological and Environmental Engineering.

Universitat Autònoma de Barcelona. 08193-Bellaterra (Spain).

*Corresponding Author: Dr. Amanda Alonso

amanda.alonso@uab.cat

Departament d'Enginyeria Química, Biològica i Ambiental.

Escola d'Enginyeria. Universitat Autònoma de Barcelona. 08193-Bellaterra (Spain).

Phone: +34 581 4793

Fax: +34 581 2013

Highlights

- Synthesized Ce-Ti oxides and Ce-Ti@Fe_3O_4 NPs were tested as adsorbents for fluoride removal from drinking water.
- Langmuir, Freundlich, and Dubbinin-Radushkevich isotherm models and mechanism estimation were evaluated.
- Ce-Ti@Fe_3O_4 NPs maximum adsorption capacity was 91 mg F/g NP.
- Regeneration and reusability of the magnetic Ce-Ti@Fe_3O_4 NPs as adsorbent were performed.
- Thermodynamic parameters for the adsorption process were calculated.

Abstract

Synthesized magnetic core-shell Ce-Ti@Fe_3O_4 nanoparticles were tested, as an adsorbent, for fluoride removal and the adsorption studies were optimized. Adsorption capacity was compared with the synthesized Ce-Ti oxide nanoparticles. The adsorption equilibrium for the Ce-Ti@Fe_3O_4 adsorbent was found to occur in less than 15 min and it was demonstrated to be stable and efficient in a wide pH range of 5-11 with high fluoride removal efficiency over 80% of all cases. Furthermore, isotherm data were fitted using Langmuir and Freundlich models, and the adsorption capacities resulted in 44.37 and 91.04 mg/g, at pH 7, for Ce-Ti oxides and Ce-Ti@Fe_3O_4 nanoparticles, respectively. The physical sorption mechanism was estimated using the Dubbinin-Radushkevich model. An anionic exchange process between the OH^- group on the surface of the Ce-Ti@Fe_3O_4 nanomaterial and the F^- was involved in the adsorption. Moreover, thermodynamic parameters proved the spontaneous process for the adsorption of fluoride on Ce-Ti@Fe_3O_4 nanoparticles. The reusability of the material through magnetic recovery was demonstrated for five cycles of adsorption-desorption. Although the nanoparticles suffer slight structure modifications after their reusability, they keep their adsorption capacity. Likewise, the efficiency of the Ce-Ti@Fe_3O_4 was demonstrated when applied to real water to obtain a residual concentration of F^- below the maximum contaminated level, 1.5 mg/L (WHO, 2006).

Keywords: magnetic core-shell nanoparticles, fluoride removal, drinking water, adsorption, reusability

1. Introduction

Fluoride contamination could be found in ground and surface water (N. Gandhi et al., 2012; Rafique et al., 2013) as well as in wastewater from fluoride chemical industries (Shen et al., 2003; Teng et al., 2009). Fluoride presents hazardous effects if it exceeds 1.5 mg/L in water (Karthikeyan et al., 2011; Singh et al., 2013; WHO, 2006) leading to various diseases (Bhatnagar et al., 2011; Liu et al., 2011; Vinati et al., 2015). The main source of these effects is from fluoride contaminated drinking water, which leads to 65% of endemic fluorosis diseases over the world (Shiklomanov, 2000; Viswanathan et al., 2009). For example, contents in drinking water of 4.8 and 1.7 mg/L in Greece and India, respectively, have been reported (Dai et al., 2004; Gupta and Kumar, 2012; Martínez-Acuña et al., 2016). Therefore, drinking water defluoridation is necessary to prevent human illness (Mohapatra et al., 2009). Defluoridation of drinking water using several technologies, including precipitation-coagulation, membrane separation process, ion exchange, electrodialysis, adsorption and reverse osmosis, had been developed (Amor et al., 2001; Chang and Liu, 2007; Meenakshi and Viswanathan, 2007; Sehn, 2008; Solangi et al., 2009; Velizarov et al., 2004). Among these methods, adsorption is the most effective, environmentally friendly, and economic method due to the simplicity of design, relatively low cost, high efficiency, and ease of operation (Bhatnagar et al., 2011). For instance, the use of biochar (Mohan et al., 2014) and biomass (Sinha et al., 2003) as adsorbent materials, were reported for fluoride removal. Furthermore, the removal of various contaminants from drinking water were performed by using nanomaterial adsorbents due to their unique properties such as large surface area, high reactivity, high specificity, and self-assembly (Qu et al., 2013). Various metal oxides and hydroxides of aluminium, iron, zirconium,

magnesium, chromium and manganese ions based nanoparticles (NPs) had been reported (Kumar et al., 2011; Lee et al., 2010; Minju et al., 2013; Sivasankar et al., 2011) for fluoride removal from water (Meenakshi and Maheshwari, 2006). Although bimetallic or mixed oxides such as Mn-Ce, Al-Ce, Zr-Mn and ceramic adsorbents were also studied for fluoride removal, some of these materials present disadvantages in terms of pH range, high cost and low adsorption capacity. (Chen et al., 2011; Deng et al., 2011; Liu et al., 2010; Sujana and Anand, 2010; Tomar et al., 2013). Thus, Zhang et al. (Zhang et al., 2015), used magnesium oxide nanomaterial for fluoride removal and it showed high adsorption capacity (about 300 mg/g) but regeneration was reported not to be favoured. V. Sivasankar et al. (Sivasankar et al., 2011), reported low adsorption capacity (9.02 mg/g) for fluoride removal from drinking water utilizing manganese dioxide based nanomaterial compared to previously reported results. Using an Al-Ce hybrid nanomaterial, Liu et al. (Liu et al., 2010) found high adsorption capacity of fluoride (91.4 mg/g), but slow kinetics to reach the equilibrium. However, to our knowledge, no studies about the reusability of the adsorbents have been reported for the reported materials (Deng et al., 2011; Liu et al., 2010). In this sense, the use of magnetic NPs for pollutants removal may provide efficient, rapid and easy separation, and especially reusability. The magnetic NPs can be either used directly as an adsorbent or as the core material in a core-shell NPs (Chai et al., 2013; Chen et al., 2012; Zhang et al., 2014). On the other hand, the hydrous Ce oxide, as rare earth metal, is reported to be more effective material for fluoride removal (46.84 mg/g) compared to other metals, although it is not useful for drinking water treatment due to its toxicity (Taylor et al., 2016). Furthermore, titanium based nanomaterials have also a great interest for fluoride removal with adsorption capacities that ranged from 15 to 47 mg/g (Chen et al., 2012; Li et

al., 2010). Therefore, mixing rare earth metals (i.e. Ce) with low-cost metals (i.e. Fe) could be advantageous for high adsorption capacities at neutral pH medium, improving the separation of the adsorbent by magnetism as well as avoiding Ce-toxicity.

Our research group was succeeded in synthesizing a new adsorbent based on magnetic core-shell Ce-Ti@Fe_3O_4 NPs (shell@core) which presented promising properties in terms of magnetism, crystalline structure and adsorption for some inorganic water contaminants (Abo Makeb et al., 2016).

In the present work, two novel nanomaterials based on Ce-Ti oxide and Ce-Ti@Fe_3O_4 NPs were synthesized and compared as adsorbents for fluoride ion removal from aqueous solution. Adsorption kinetics, isotherms and the effect of different parameters (i.e. pH and temperature) in the adsorption capacity of the materials were studied. Also, the use of the Ce-Ti@Fe_3O_4 NPs for the treatment of real drinking water was performed. Further, the reuse of the Ce-Ti@Fe_3O_4 adsorbent was evaluated.

2. Materials and methods

2.1. Materials

Iron (II) chloride ($FeCl_2$, 98 %), iron (III) chloride hexahydrate ($FeCl_3 \cdot 6H_2O$, ≥ 99 %), sodium fluoride (NaF, ≥ 99 %), titanium chloride ($TiCl_4$, ≥ 99.98 %), cerium nitrate hexahydrate ($Ce(NO_3)_3.6H_2O$, ≥ 99 %), and ammonia solution were purchased from Sigma-Aldrich, Spain. Sodium hydroxide pellets (NaOH), was purchased from Merk. Hydrochloric acid (HCl), and cetyltrimethylammonium bromide (CTAB) were purchased from Panreac, SA. All the chemicals were of analytical grade or higher, and all solutions were prepared with Milli-Q water and filtered using 0.45 μm Nylon membrane filter.

2.2. Preparation of the Ce-Ti oxide nanoparticles and Ce-Ti@Fe_3O_4 nanoparticles

This synthetic procedure for Ce-Ti oxide NPs was adapted from similar works about core-shell magnetic Ti-NPs synthesis (Zhang et al., 2014). Briefly, in this work, $TiCl_4$ and $Ce(NO_3)_3 \cdot 6H_2O$ were dissolved in Milli-Q water and mixed at 25 °C. Then 12.5 % NH_3 solution was slowly added dropwise untill pH 7.0 was reached. Then, the Ce-Ti NPs produced were washed, centrifuged and dried. Detailed information about the methodology is reported in the Supporting Information (SI.1).

The Ce-Ti@Fe_3O_4 NPs were prepared by the co-precipitation method reported by our research group (Abo Makeb et al., 2016) (detailed information is provided in SI.1).

2.3. Characterization of the nanomaterials

Inductively Coupled Plasma Optical Emission Spectrometry (ICP-OES) was used for the metal concentration analysis of both synthesized nanomaterials. The detailed sample preparation for ICP-OES analysis is in SI.2.1. Also, High-Resolution Transmission Electron Microscopy (HRTEM) coupled with Energy-Dispersive Spectroscopy (EDS), and Electron Diffraction (ED) Pattern were acquired using a JEM-2011/ JEOL microscope operated at 200 kV and equipped with an INCA X-MAX detector. HRTEM was used to characterize the morphology and sizes of both Ce-Ti@Fe_3O_4 and Ce-Ti oxide NPs and, EDS and ED were used to analyze the composition and the crystalline structure (SI.3). The morphology of the NPs was determined by Scanning Transmission Electron Microscopy (STEM) coupled with high-angle annular dark field (HAADF) detector and Electron Energy Loss Spectra (EELS).

144 2.3. *Adsorption and desorption experiments procedure*

145 For all the experiments, batch adsorption tests were used to determine the fluoride
146 adsorption efficiency of both synthesized NPs. A dose of adsorbent (W) (g/L) was added
147 into a conical flask containing fluoride solution with an initial fluoride concentration (C_0).
148 Typically, 25 mg of the adsorbent was added into the conical flask, which contains 25 mL
149 of the fluoride ion solution, C_0. Depending on the experiment, pH of the solution was
150 adjusted using NaOH or HCl, both at 0.1 M. The flask was shaken (200 rpm) at 25 °C
151 using a thermostatic shaker. Residual fluoride concentration in the solution, C_e, was
152 determined by ionic chromatography by using ICS-2000 (Dionex) system (SI.4).
153 Equilibrium adsorption capacity, Q_e, of the adsorbent was calculated as Eq. 1:

154

155 $$Q_e = (C_0 - C_e)/\mathrm{W} \qquad (1)$$

156

157 *2.3.1. Adsorption isotherms*

158 Adsorption isotherm experiments of both synthesized Ce-Ti oxides and Ce-Ti@Fe_3O_4 NPs
159 were performed at different concentrations of fluoride from 1 to 500 mg/L at pH 7 with an
160 adsorbent amount of 1 g/L and treated, as described in section 2.3.1, for 60 min, to assure
161 to reach the equilibrium. Then, residual fluoride concentrations were measured after
162 filtration using 0.45 μm Nylon membrane filter. All experiments were performed in
163 triplicate. Detailed information of the adsorption isotherm models is provided in SI.5.

164

165 *2.3.2. Fluoride desorption procedure*

Different studies proved that the most effective desorbing reagent for regeneration of the adsorbent is the NaOH solution (Mahramanlioglu et al., 2002; Zhang et al., 2005). The desorption experiments were performed after adsorption of 10 mg/L of fluoride using 1.0 g/L of Ce-Ti@Fe_3O_4 NPs for 60 min at pH 7.0, by shaking the adsorbent at 200 rpm using two different concentrations and volumes of NaOH desorbing solution: 25 mL of 0.5 M NaOH, and 5 mL of 0.1 M NaOH, at intervals of time of 2, 4, 6, 8, and 12 h. Then, the fluoride concentrations of the desorbing solutions were analyzed as previously mentioned.

2.3.3. Reusability of the Ce-Ti@Fe_3O_4 NPs as adsorbent and characterization

Under the optimized conditions for desorption, five cycles of the adsorption-desorption processes were performed for evaluating the reusability of the synthesized NPs for fluoride removal and its recovery. The composition, morphology, and size of the Ce-Ti@Fe_3O_4 NPs were analyzed after its use for five adsorption-desorption cycles and compared to the original material (SI2 and SI6). TEM images were obtained to analyze the size and NPs distribution and EELS spectra (SI.6) were obtained after the use of Ce-Ti@Fe_3O_4 NPs for 5 cycles of adsorption-desorption of fluoride.

Moreover, the possibility of Ce releases from the Ce-Ti@Fe_3O_4 NPs after its use was determined by Inductively Coupled Plasma Mass Spectrometry (ICP-MS) either in the treated water or in the regenerating solution, after each adsorption-desorption cycle. The detailed sample preparation and analysis for ICP-MS analysis is explained in SI.2.2.

2.3.4. pH effect on the adsorption capacity

The effect of the pH value in the media for fluoride adsorption was conducted using 10 mg/L initial fluoride concentration with 1 g/L of Ce-Ti@Fe_3O_4 adsorbent. Then, each conical flask at fixed pH of 5, 7, 9 and 11 was shaken and the adsorption capacity was calculated. All experiments were performed in triplicates.

2.3.5. Effect of temperature on the fluoride adsorption and estimation of the thermodynamic parameters

The effect of the temperature on the fluoride adsorption onto Ce-Ti@Fe_3O_4 adsorbent was studied at 20, 25, 30, 35, and 40 °C using 30 mg/L of fluoride initial concentration at pH 7 with 1 g/L adsorbent dose, 60 min contact time, and 200 rpm shaking. The adsorption capacity was calculated in all the cases. To estimate the effect of temperature on the adsorption of fluoride onto Ce-Ti@Fe_3O_4 NPs, the free energy Gibbs change ($\Delta G°$), enthalpy change ($\Delta H°$), and entropy change ($\Delta S°$) were determined as previously reported (Zhao et al., 2010). In this method, the thermodynamic parameters were obtained directly from the plot of $\log(Q_e/C_e)$ versus 1/T as presented in Eq. 2 and 3.

$$\ln\left(\frac{Q_e}{C_e}\right) = \left(\frac{\Delta H^\circ}{R}\right) - \left(\frac{\Delta S^\circ}{R}\right)\frac{1}{T} \qquad (2)$$

$$\Delta G^\circ = \Delta H^\circ - T\Delta S^\circ \qquad (3)$$

Where Q_e/C_e is the adsorption affinity; $\Delta G°$, $\Delta H°$ and $\Delta S°$ are the change in free energy, enthalpy, and entropy respectively. All experiments were performed in triplicates.

2.3.6. Fluoride removal from spiked drinking water by using Ce-Ti@Fe_3O_4 NPs

To determine the effect of the presence of other ions on the removal of fluoride, drinking tap water was spiked only with 10 mg/L of fluoride. Tap water samples were obtained from

211 the Universitat Autònoma de Barcelona (Spain). Drinking tap water first was turned on a
212 steady stream with flow 500 mL/min and run for 10 min to remove any stagnant in the
213 plumbing network. The adsorption experiment was carried out at pH 7.0 in 250 mL flasks
214 containing 0.10 g Ce-Ti@Fe_3O_4 adsorbents per 100 mL of spiked water, at 25 and 30°C,
215 and shaking at 200 rpm for 60 min.
216
217 *2.3.7. Statistical data analysis*
218 Statistical analysis was performed using the Tukey's method based on one factor ANOVA
219 at the 5% confidence level using SPSS 15.0.1 (SPSS Inc., USA). Statistically significant
220 differences were reported when the probability of the results, assuming the null hypothesis
221 (p) value is less than 0.05.
222
223 **3. Results and discussion**
224 *3.1. Characterization of the synthesized nanomaterials*
225 The metal content of the synthesized Ce-Ti oxides NPs was analyzed using ICP-OES. The
226 results showed the presence of 84.99±5.05 mg_{Ti}/g_{NP} (1.8 $mmol_{Ti}/g_{NP}$) and 106.93±3.54
227 mg_{Ce}/g_{NP} (0.8 $mmol_{Ce}/g_{NP}$) at the synthesis conditions. This means that the synthesized
228 nanomaterial contains the desired metals and that the molar ratio of Ce:Ti was 1:2.
229 Comparing with the previous characterized Ce-Ti@Fe_3O_4 nanomaterial, Ce:Ti:Fe molar
230 ratio was 1:2:1 (Abo Makeb et al., 2016). Thus, the incorporation of Fe into the Ce-Ti
231 oxide NPs did not affect the metals molar ratio in the final Ce-Ti@Fe_3O_4 adsorbent.
232 Further, morphological characterization of the Ce-Ti oxides was also studied. Fig. 1
233 illustrates the TEM images coupled with EDS and SAED pattern for Ce-Ti oxide NPs. As

shown in Fig. 1a, Ce-Ti oxide NPs size is estimated to be about 1-2 nm, much smaller than the Ce-Ti@Fe_3O_4 NPs (10 – 15 nm) probably due to the addition of Fe_3O_4 core in the structure that induces an increase of the total NPs size.

The SAED pattern for Ce-Ti oxides NPs (Fig. 1b) exhibit no crystal orientation (as no bright dots or rings are observed) and hence, amorphous structure (Martos et al., 2008). Conversely, the SAED pattern for Ce-Ti@Fe_3O_4 NPs sample (Fig. S1, S2), exhibited a poly-nanocrystalline structure which corresponds to magnetite NPs (Wang et al., 2013).

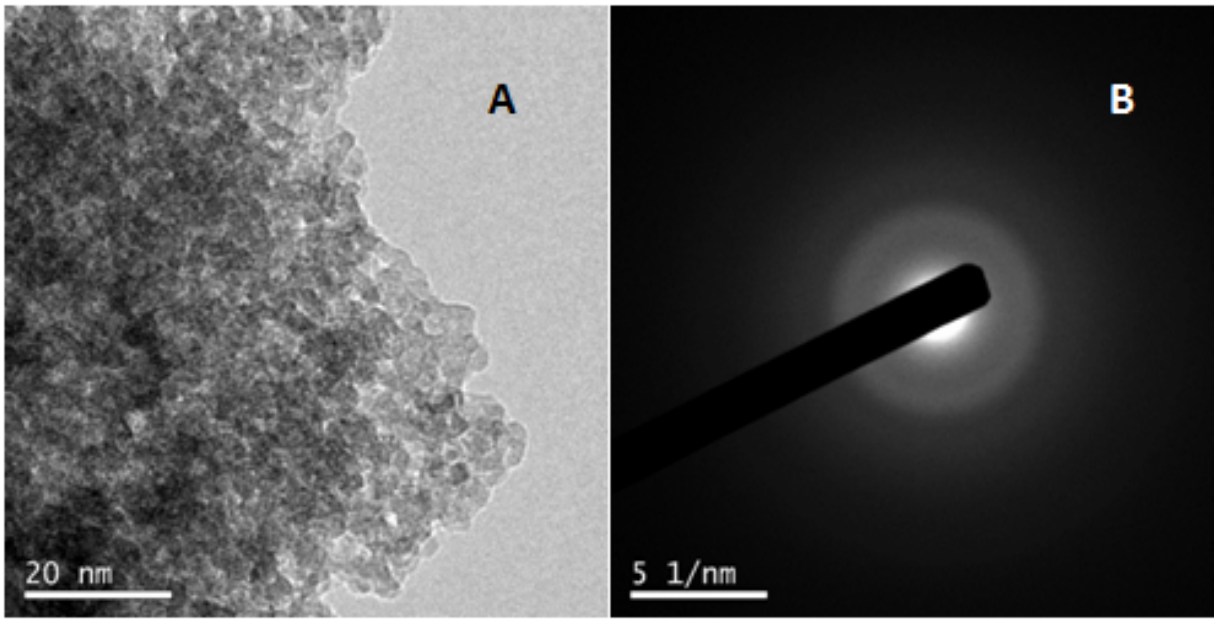

Fig. 1. (A) HRTEM image and, (B) SAED pattern of Ce-Ti oxide NPs.

3.2. Fluoride adsorption on Ce-Ti@Fe_3O_4 adsorbents

The time required to achieve the equilibrium for the fluoride adsorption was determined at 10 and 100 mg/L of fluoride and an adsorbent dose of 1 g/L of Ce-Ti@Fe_3O_4 NPs at pH 7 and 25°C. The equilibrium time was reached at 0.5 min for 10 mg/L and at 15 min for 100 mg/L of initial fluoride concentration. These results showed a high adsorption rate for the

synthesized nanomaterial. Therefore, to assure the completed adsorption of the contaminant, the adsorption time was fixed to be 60 min for the rest of the batch experiments. The fast kinetics of this novel adsorbent could be attributed to a large number of available adsorption sites on the Ce-Ti@Fe_3O_4 adsorbent surface. Moreover, the presence of Ce in the Ce-Ti@Fe_3O_4 NPs enhanced the adsorption time compared with the reported one Fe-Ti@Fe_3O_4 (Zhang et al., 2014) under the same conditions. Further explanation about the improved adsorption mechanism of the Ce-Ti@Fe_3O_4 NPs is following discussed.

3.2.1. *Adsorption isotherms and modeling for the adsorption mechanism*

Maximum adsorption capacity was estimated from the adsorption isotherm models by performing the experiments over the fluoride initial concentration range until saturation at pH 7. A broad range of initial fluoride concentration (1 to 500 mg/L) was selected to ensure saturation and allow isotherm fitting. Fig. 2 corresponds to the adsorption isotherms for both, Ce-Ti oxides and Ce-Ti@Fe_3O_4 NPs. It is shown that the adsorption capacities of both nanomaterials increased with increasing fluoride concentrations, and maximum values were achieved at the equilibrium fluoride concentration above 100 mg/L.

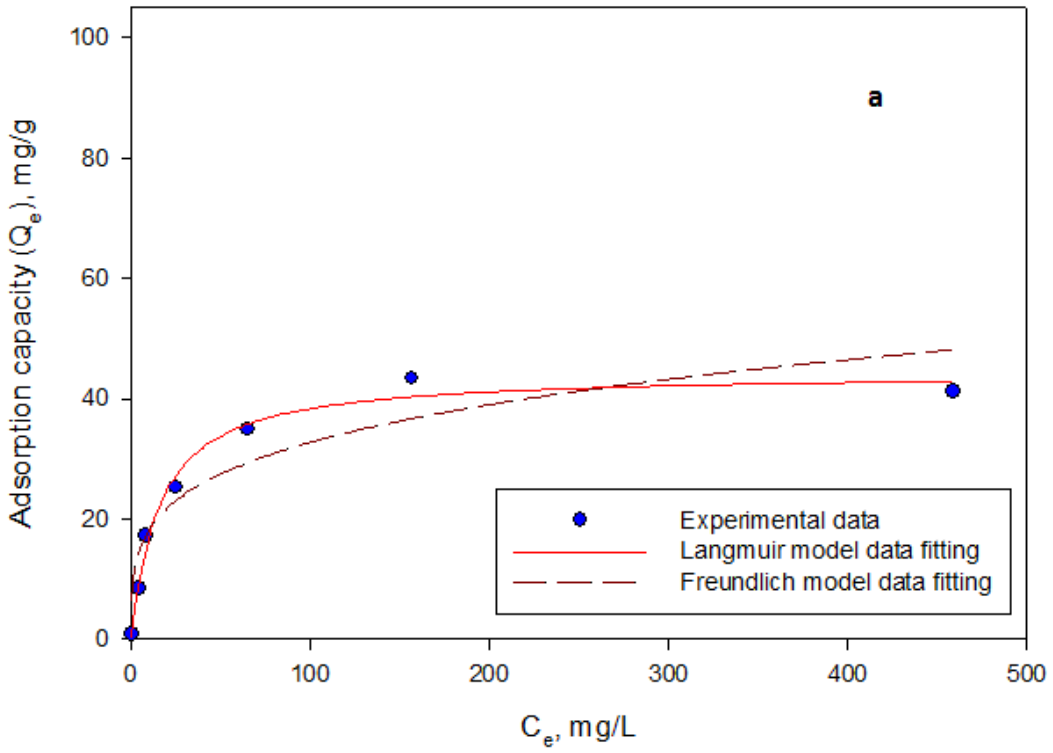

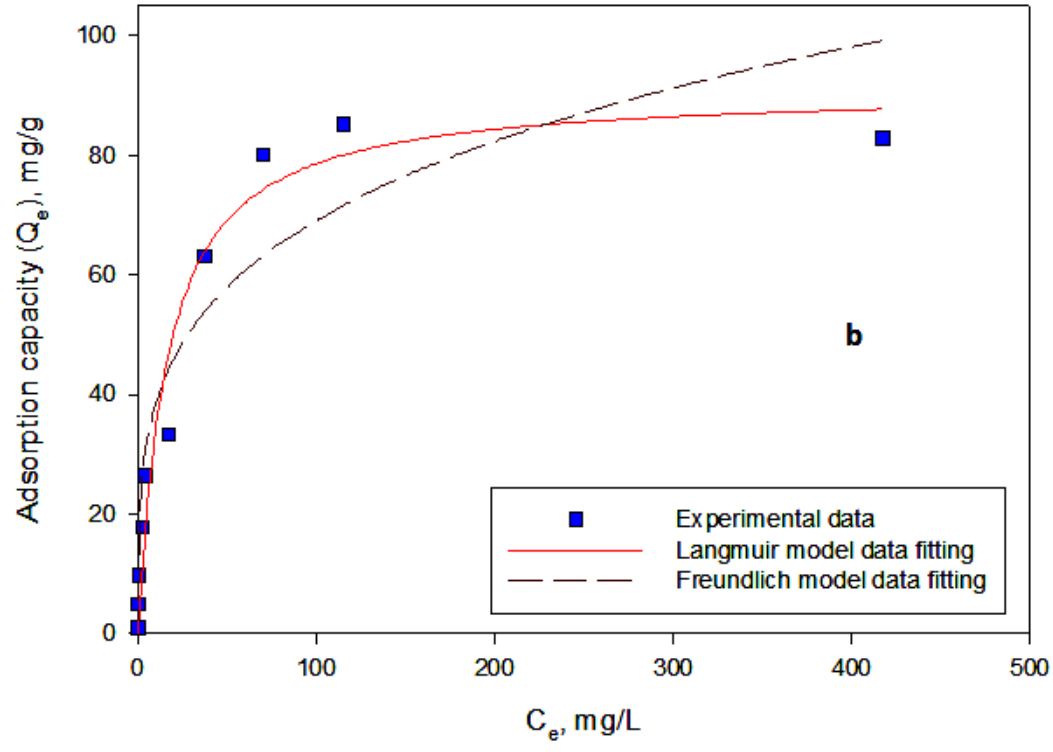

Fig. 2. Adsorption isotherms and experimental data fitting using Langmuir and Freundlich models for fluoride removal using: (a) Ce-Ti oxide, and (b) Ce-Ti@Fe_3O_4 NPs [adsorbent dose 1 g/L, 60 min shaking at 200 rpm at room temperature].

Furthermore, data were fitted to both Langmuir and Freundlich models (Table 1). The Langmuir model seems to be more suitable for fluoride adsorption than the Freundlich one as Langmuir model regression coefficient (R^2) was higher than 0.95. However, it is possible to obtain mechanistic information on the adsorption process from both models. The maximum monolayer adsorption capacity (Q_m) obtained for Ce-Ti@Fe_3O_4 NPs was 91.04 mg/g, higher than for Ce-Ti oxide NPs (Q_m = 44.37 mg/g). The Freundlich adsorption intensity parameter (n values) were higher than 2, also supporting the favorable adsorption of fluoride and meaning that the sorption process is mainly physical rather than chemical.

Table 1. Langmuir, Freundlich, and Dubinin–Radushkevich isotherms for fluoride adsorption onto Ce-Ti oxides and Ce-Ti@Fe_3O_4 NPs

Isotherm models		**Nanomaterial**	
		Ce-Ti@Fe_3O_4	**Ce-Ti oxide**
Langmuir	**Q_m (mg/g)**	91.04	44.37
	K_L (L/mg)	0.063	0.064
	R^2	0.952	0.986
Freundlich	**K_F ($mg^{1-(1/n)}L^{1/n}g^{-1}$)**	21.543	10.214
	n	3.95	3.95
	R^2	0.895	0.877
D-R	**Q_m (mg/g)**	83.86	37.14
	K_{DR} (mol^2/kJ^2)	4.77e-5	8.05e-6
	R^2	0.887	0.895
	E (kJ/mol)	0.102	0.250

The calculated parameter of the energy, E, of the Dubinin–Radushkevich isotherm (SI.6) is indicated in Table 1. The E values were 0.10 and 0.25 kJ/mol for Ce-Ti@Fe_3O_4 and Ce-Ti oxides adsorbents, respectively, which proved that the interaction between the fluoride and

288 the surface of the nanomaterials is physical (Babaeivelni and Khodadoust, 2013; Dorado et
289 al., 2010). The lower E value for Ce-Ti@Fe_3O_4 means that it needs lower energy for
290 adsorbing F^- than Ce-Ti oxides NPs. It confirms its higher adsorption capacity. Fluoride
291 removal may suffer a surface ion-exchange process as physisorption based on the exchange
292 of the hydroxyl ions (OH^-) from the surface of the adsorbent with F^- (Abo Makeb et al.,
293 2016). The OH^- on the surface of the NPs is present due to the nature of the media (e.g. pH)
294 (Pattanaik and Bhaumik, 2000). According to Zhang et al. (2015), the physical mechanism
295 could be expressed by Eqs. 2 and 3:

296 $$M^{n+} + nH_2O \rightarrow M(OH)_n \quad (2)$$

297 $$M(OH)_n + xF^- \rightarrow M(OH)_{n-x}F_x + xOH^- \quad (3)$$

298

299 Where M, n, and x are the adsorbent's metal ion, the valence of the metal ion and, the
300 number of moles of fluoride, respectively.
301 Further, it is worth to mention that the crystalline structure of the adsorbents plays an
302 important role in the adsorption capacity. As shown, the crystalline Ce-Ti@Fe_3O_4 material
303 showed higher adsorption capacity than the amorphous Ce-Ti oxide due to the higher
304 developed crystalline faces of the NPs which could increase the ability of the surface to
305 adsorb (Giammar et al., 2006).
306 Fluoride adsorption capacity using the novel Ce-Ti oxides and Ce-Ti@Fe_3O_4 NPs is highly
307 competitive in comparison with other adsorbents from literature (Table 2). The Q_{max} of the
308 adsorbents in this study is similar to the best ones reported so far. However, those materials
309 present some disadvantages in comparison with the Ce-Ti@Fe_3O_4 adsorbent. For instance,
310 Mn–Ce oxide and the Fe_3O_4@$Al(OH)_3$ adsorbents reached the equilibrium after 3 h and 60

311 min, respectively (Deng et al., 2011; Zhao et al., 2010). The new developed nanomaterial,
312 Ce-Ti@Fe_3O_4, presents promising properties in terms of adsorption capacity, adsorption
313 rate, as well as magnetic properties and, consequently, Ce-Ti@Fe_3O_4 nanomaterial was
314 used for the rest of the experiments.
315
316 **Table 2.** Comparison of adsorption capacity of fluoride on different nanomaterials
317 from this work and the literature. "Maximum adsorption capacity" indicates that the
318 value of Adsorption capacity was obtained through an isotherm modelling.

Adsorbents	**Adsorption capacity (mg/g)**	**sorbent/ sorbate ratio**	**Adsorption conditions**	**Reference**
Fe_3O_4@ZrO_2	158.60	Maximum adsorption capacity	deionized water, 25 °C, adsorption time 1 h, pH 2.5, adsorbent dose 1 g/L	Riahi et al., 2015
Ce-Ti@Fe_3O_4 powder	91.04	Maximum adsorption capacity	deionized water, 25 °C, adsorption time 1 h, pH 7.0, adsorbent dose 1.0 g/L	This work
Fe_3O_4@$Al(OH)_3$	88.48	Maximum adsorption capacity	deionized water, 25 °C, adsorption time 1 h, pH 6.5, adsorbent dose 1 g/L	Zhao et al., 2010
Powder Mn-Ce oxide	79.50	Maximum adsorption capacity	deionized water, 25 °C, adsorption time 24 h, pH 6.0, adsorbent dose 0.01 g/L	Deng et al., 2011
Ce-Fe bimetal oxides	60.97	Maximum adsorption capacity	deionized water, 20 °C, adsorption time 1 h, pH 5.5,	Tang and Zhang, 2016

			adsorbent dose 0.5 g/L	
Fe-Ti@Fe_3O_4	57.22	Maximum adsorption capacity	deionized water, 25 °C, adsorption time 12 h, adsorbent dose 1 g/L	Zhang et al., 2014
Iron-doped titanium oxide	53.22	Maximum adsorption capacity	deionized water, 25 °C, adsorption time 12 h, pH 5.0, adsorbent dose 0.5 g/L	Chen et al., 2012
Fe-Ti bimetallic oxide	47.00	Maximum adsorption capacity	deionized water, 25 °C, adsorption time 12 h, pH 5.0, adsorbent dose 0.5 g/L	Chen et al., 2012
Ti-La hybrid	46.60	Maximum adsorption capacity	deionized water, 25 °C, adsorption time 12 h, pH 6.0, adsorbent dose 0.01 g/L	Li et al., 2010
Granular Mn-Ce oxide	45.50	Maximum adsorption capacity	deionized water, 25 °C, adsorption time 24 h, pH 6.0, adsorbent dose 0.01 g/L	Deng et al., 2011
Ce-Ti oxide powder	44.37	Maximum adsorption capacity	deionized water, 25 °C, adsorption time 1 h, pH 7.0, adsorbent dose 1.0 g/L	This work
Fe-Ti/Fe_3O_4	41.80	Maximum adsorption capacity	deionized water, 25 °C, adsorption time 12 h, pH 7.0, adsorbent dose 1.0 g/L	Zhang et al., 2016
Ti-Ce hybrid	30.60	Maximum adsorption capacity	deionized water, 25 °C, adsorption time 12 h, pH 6.0,	Li et al., 2010

			adsorbent dose 0.01 g/L	
$TiOH_4$	30.40	Maximum adsorption capacity	deionized water, 25 °C, adsorption time 12 h, pH 5.0, adsorbent dose 2.0 g/L	Ishihara et al., 2002
CeO_2-TiO_2/SiO_2	21.40	Maximum adsorption capacity	deionized water, 35 °C, adsorption time 1 h, pH 4.0, adsorbent dose 5.0 g/L	Y. Xiuru et al., 1998
Fe-Al	17.70	Maximum adsorption capacity	deionized water, 30 °C, adsorption time 12 h, pH 6.8, adsorbent dose 0.1 g/L	Biswas et al., 2007
Fe-Cr	16.34	Maximum adsorption capacity	deionized water, 25 °C, adsorption time 1.5 h, pH 6.5, adsorbent dose 0.1 g/L	Biswas et al., 2010
Fe-Sn	10.50	Maximum adsorption capacity	deionized water, 30 °C, adsorption time 2 h, pH 6.4, adsorbent dose 0.1 g/L	Biswas et al., 2009
Fe-Zr	8.20	Maximum adsorption capacity	deionized water, 30 °C, adsorption time 12 h, pH 6.8, adsorbent dose 0.1 g/L	Biswas et al., 2007
Aluminium modified zeolite tuff	3.24	Maximum adsorption capacity	deionized water, 30 °C, flow rate 1 mL/min, bed height 4 cm, pH 6.2, adsorbent dose 1 g/L	Teutli-Sequeira et al., 2015
Fe_3O_4	0.30	20.00	deionized	Zhang et

			water, 25 °C, adsorption time 12 h, adsorbent dose 1 g/L	al., 2014

319

320

321 *3.3. Evaluation of the fluoride recovery and the reusability of the Ce-Ti@Fe_3O_4 NPs*

322 The efficiency of the adsorbent is demonstrated by performing adsorption-desorption
323 cycles of 10mg/L of F^- for evaluating the reuse and regeneration of the adsorbent. Ce-
324 Ti@Fe_3O_4 was separated from the treated solution by a magnet (Abo Makeb et al., 2016).
325 In this work, it was shown that the recovery percentage of fluoride was affected by
326 desorption time (ANOVA analysis, $p < 0.05$). As shown in Fig. 3, by using 5 mL of 0.1 M
327 NaOH, it was obtained the highest recovery percentage of 98.51 % at 12 hours of
328 desorption time (Fig. 3b) which were the chosen desorption conditions for each
329 regeneration step due to low concentration and volume of NaOH. However, the little
330 decrease of the recovery percentage of fluoride at 8 h desorption using 0.5 M NaOH could
331 be attributed to a saturation of the fluoride recovery after 6 h desorption time.

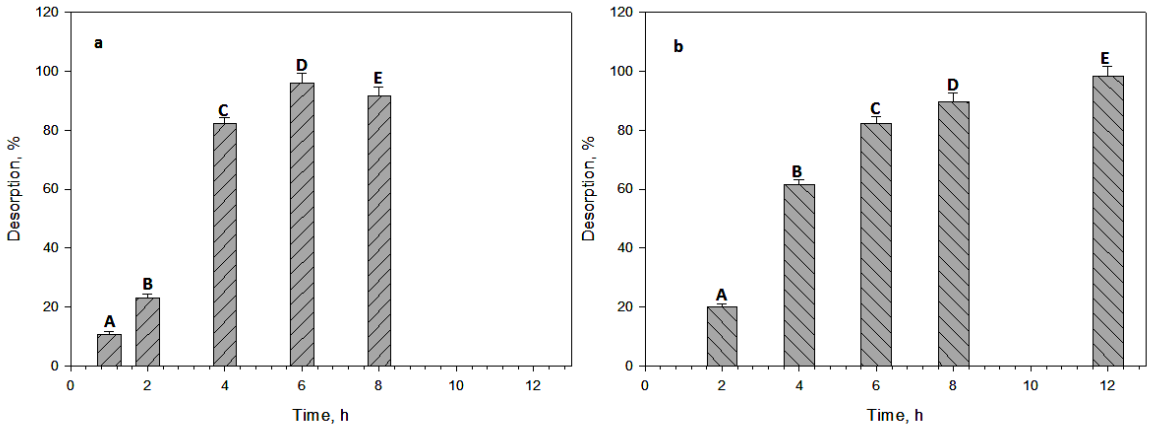

332

333 **Fig. 3.** The effect of the desorption time for the efficient fluoride desorption (%); (a) 25 mL of
334 0.5M NaOH and, (b) 5 mL of 0.1M NaOH, using 1 g/L of Ce-Ti@Fe_3O_4 nanomaterial, and

shaking at 200 rpm. Statistical data analysis using ANOVA was illustrated by letters A, B, C, D, and E.

The reusability of the Ce-Ti@Fe_3O_4 adsorbent was carried out by performing five consecutive adsorption-desorption cycles under both optimal experimental conditions were obtained for both processes. Thus, Fig. 4 illustrates the adsorption capacities values of the Ce-Ti@Fe_3O_4 adsorbent and the fluoride recovery versus the cycle's number. It is shown that the fluoride recovery % is high (> 90%) for all the cycles tested and also in comparison with other reported works, where the maximum fluoride recovery has been up to 86.35 % (Zhang et al., 2015). Also, a very little decrease in the recovery exists from the first to the fifth cycle to be from 98.51 to 92.97% that could be attributed to the change of the morphology of the NPs or because of the metal release from the adsorbent during the regeneration process, as it is following discussed. However, the high removal % in all the cycles was demonstrated.

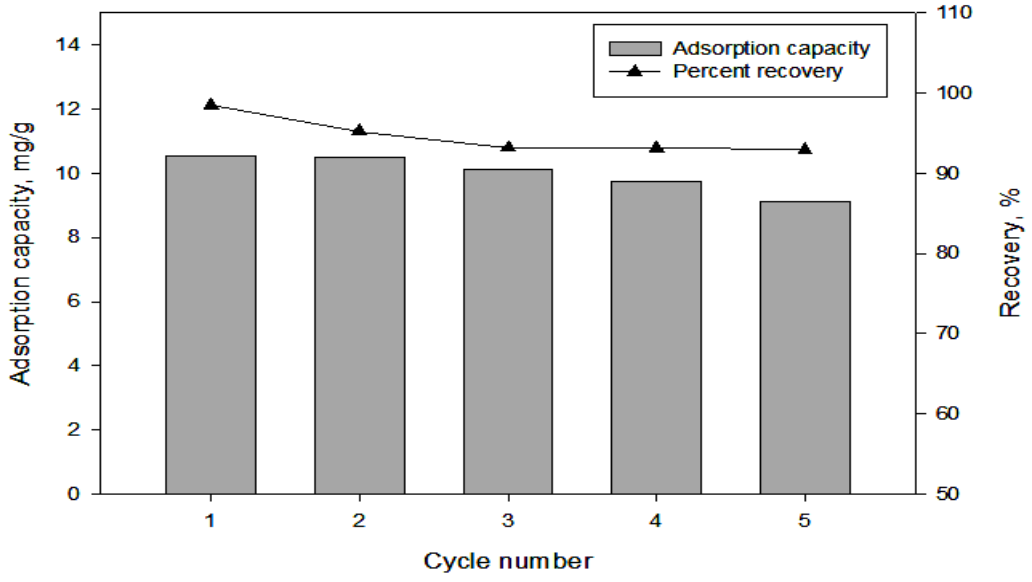

Fig. 4. Fluoride adsorption capacities (mg/g) and fluoride recovery (%) for the use of Ce-Ti@Fe_3O_4 NPs at different adsorption-desorption cycles (up to 5).

352

353 *3.4. Characterization of the Ce-Ti@Fe_3O_4 NPs as adsorbent after reuse*

354 Fig. 5a illustrates the TEM image of the corresponding Ce-Ti@Fe_3O_4 adsorbent after its
355 use for five cycles of the adsorption-desorption process. It is shown an aggregation of the
356 NPs in comparison with the size of the original NPs, leading to an increase of the size and
357 hence, a decrease on the adsorption capacity. In this sense, Fig. 5b showed the SAED
358 pattern of the adsorbent and it showed a decrease in the crystalline phases in comparison
359 with the original adsorbent (SI.2). As discussed in Section 3.1, the loss of the crystalline
360 structure may affect the adsorption efficiency of the nanomaterial.

361

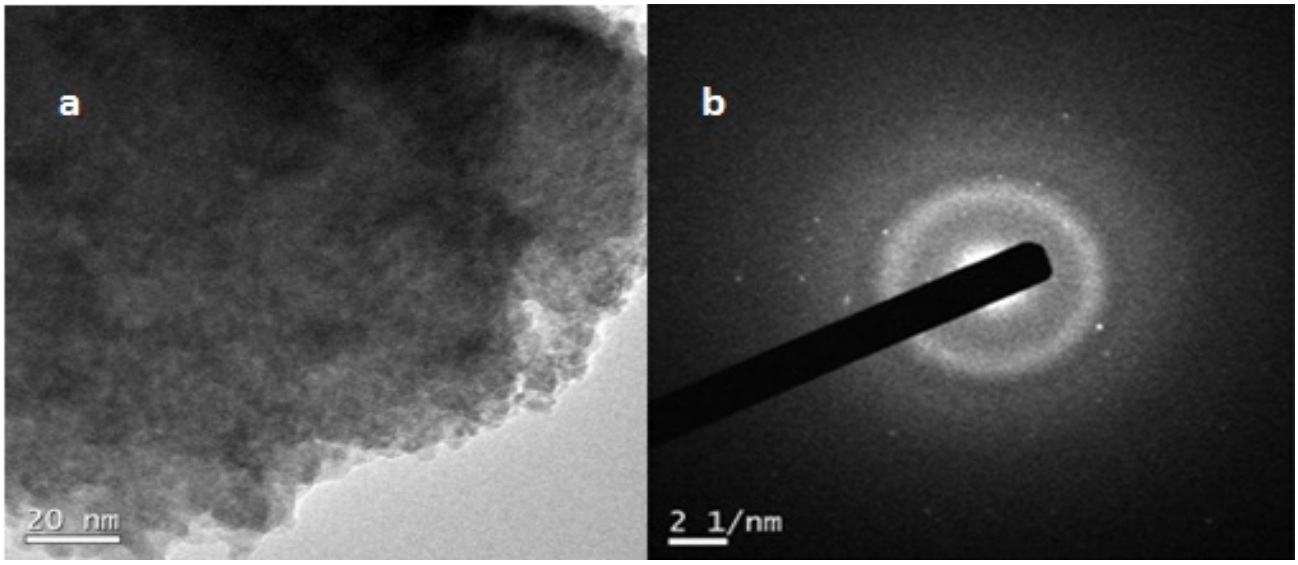

362

363 **Fig. 5.** TEM image (a) and, ED pattern (b) of the Ce-Ti@Fe_3O_4 nanomaterial after five
364 adsorption-desorption cycles under the optimal experimental conditions used for each process.

365

366 Furthermore, the core-shell structure of the original Ce-Ti@Fe_3O_4 nanomaterial is shown in
367 SI.2 and SI.6. Here, the STEM-EELS technique was used to characterize the NPs structure
368 after it is used and a slight modification of the core-shell structure, due to its aggregation, is

shown (HAADF image, Fig. 6a). Moreover, the elemental analysis of the three metals was proved using STEM-based EDS (Fig. 6b and 6c**)** and thus, the metal composition remains stable in the NPs' structure. Anyway, the nanomaterial still presents magnetic properties and high adsorption activity after its reuse.

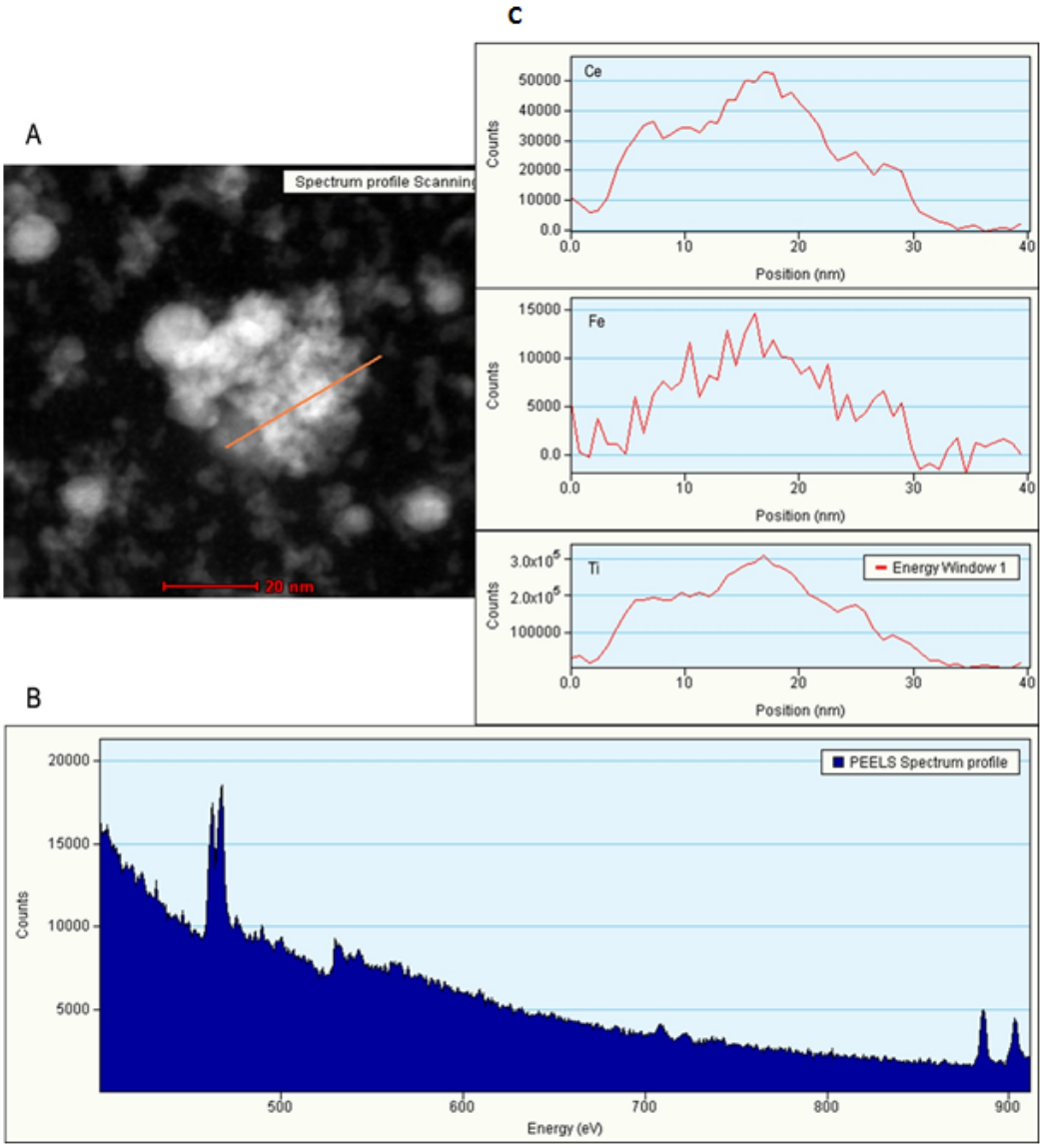

Fig. 6. EELS line scan of the core-shell Ce-Ti@Fe_3O_4 NPs after the 5 cycles of adsorption-desorption. (A) STEM HAADF image of the Ce-Ti@Fe_3O_4 and position of the line scan; (B) PEELS spectrum of the nanomaterial; and (C) Ions profile spectra along the line scanning.

The observed modification of the morphology for the nanomaterial may be attributed to the release of metal. As a result, the analysis of the metal content in the Ce-Ti@Fe_3O_4 nanomaterial after the 5 cycles showed a metal concentration of 113.68±1.75 mg_{Ti}/g_{NP}, 173.82± 15.73 mg_{Ce}/g_{NP} and 77.41 ± 8.04 mg_{Fe}/g_{NP}. Comparing with the original metal values of the Ce-Ti@Fe_3O_4 NPs, (121.01±7.70 mg Ti/g, 199.29±10.47 mg Ce/g and 81.07±4.49 mg Fe/g), a leakage of Ti, Ce, and Fe of 6.06, 12.78, and 4.51%, respectively, is observed, being the loss of Ce the most important one. Then, ICP-MS was used to analyze the Ce amount in both, the water treated and the desorbing solutions, after each adsorption-desorption cycle. The Ce concentration in the final treated aqueous solution after 5 cycles was not detected (Table 3), indicating that there is no release of Ce in the treated aqueous solution. However, the Ce concentration in the desorbing NaOH solution increases with the number of desorbing cycles, being the maximum value at the 5^{th} cycle and corresponding to a total Ce release of 0.70 mg, which agrees with the estimated Ce lose from the NPs (12.78 %). This result may be due to the low stability of the NPs at basic pH (Tso et al., 2010).

Table 3. ICP-MS analysis for Ce-Ti@Fe_3O_4 after 5 adsorption-desorption cycles of fluoride

Desorption cycles, solution analyzed	**Cerium, mg/L**
Cycle 1, H_2O	N.D
Cycle 1, NaOH	N.D
Cycle 2, NaOH	N.D
Cycle 3, NaOH	0.36
Cycle 4, NaOH	10.20
Cycle 5, NaOH	20.00

Cycle 5, H_2O	N.D

N.D: Not detected

Therefore, we can conclude that the Ce-Ti@Fe_3O_4 nanomaterial is suitable for its use and reuse for at least five cycles of adsorption-desorption of fluoride with high removal and recovery. Also, it was demonstrated its adsorption capacity for five cycles. Although, there is a low metal leakage from the nanomaterial, there is no effect in the treated water or the environment, due to this leakage remains in the desorbing reagent.

3.4.Effect of the pH value for the fluoride adsorption.

The optimum pH for drinking water is in the range of 6.5–9.5 (Drinking-water, 2004) and it is known that pH can significantly affect the adsorption of fluoride (Habuda-Stanić et al., 2014). Fig. 7 shows the removal percentage and adsorption capacity (Q_e) at pH from 5 to 11 for the Ce-Ti@Fe_3O_4 adsorbent. The fluoride removal percentage and Q_e decrease by increasing the pH when applying 10 mg/L initial fluoride concentration and 1 g/L of Ce-Ti@Fe_3O_4 NPs. Even though, at pH 11, the removal percentage was still more than 80 %. The decrease of the removal percentage could be attributed to the changes in the surface of the NPs, which became more negatively charged. Therefore, a competition for the adsorption sites of more OH^- ions with fluoride ions occurs in the aqueous solution as well as modifications of the nanomaterial in this pH range (Raichur and Jyoti Basu, 2001). At 10 mg/L F^- initial concentration, the highest fluoride removal percentage and Q_e values were at pH 5 and 7 to be 99.85, 98.33 % and 10.31, 10.32 mg/g, respectively.

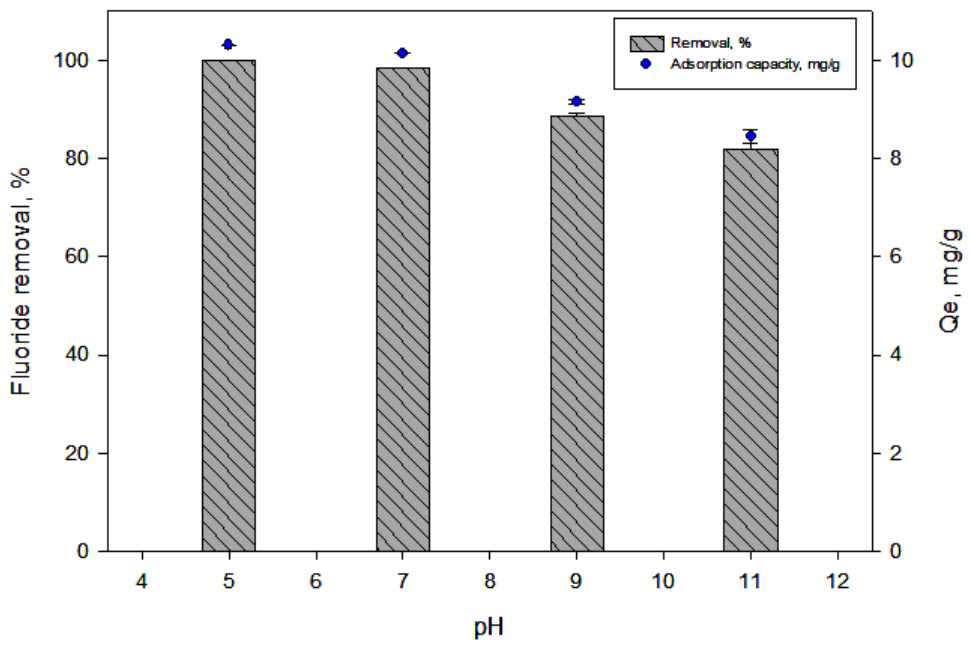

415

416 **Fig. 7.** Effect of pH on fluoride removal percentage (%) and adsorption capacity (Qe) for
417 initial fluoride concentration of 10 mg/L, 1 g/L of Ce-Ti-Fe oxides NP at 200 rpm and room
418 temperature.

419

420 *3.5 Temperature effect and thermodynamic parameters*

421 The temperature affects the adsorption of the pollutants and provides information about the
422 spontaneity of the fluoride removal process (Deniz, 2013). The adsorption capacity values
423 using Ce-Ti@Fe_3O_4 NPs and fluoride removal percentage are illustrated in Fig. 8 versus
424 temperature in the range of 20 – 40 °C. The highest adsorption capacity is reached at 30 °C.
425 Next, the values showed a stable removal percentage until 40 °C that indicates that the
426 optimum temperature for fluoride adsorption is at 30 °C when using 30 mg/L initial
427 fluoride concentration.

428 Table 4 shows the thermodynamic parameters for the fluoride removal at different
429 temperatures. The positive value of the enthalpy, $\Delta H°$, verifies the endothermic nature of
430 the process. The positive entropy, $\Delta S°$, values confirmed the increased randomness at the

solid–solute interface during adsorption, but its low value indicated that no remarkable change in entropy occurs. Moreover, the negative free Gibbs energy, ΔG^{o}, values attributed to the adsorption processes, were spontaneous in all cases. The spontaneity adsorption process of fluoride was enhanced by increasing the temperature. The statistical analysis also showed that the temperature has a significant effect on the removal percentage of fluoride when applying the one-way ANOVA (p-value was less than 0.05) as illustrated in Fig. 8.

Table 4. Thermodynamic parameters for fluoride adsorption using Ce-Ti@Fe_3O_4 nanomaterial

Temperature (°C)	**- ΔG (kJ mol^{-1})**	**ΔH° (kJ mol^{-1})**	**ΔS° (J mol^{-1}K^{-1})**	**R^2**
20	13.84 ± 0.02	2.52	55.79	0.996
25	14.12 ± 0.02			
30	14.40 ± 0.01			
35	14.67 ± 0.04			
40	14.95 ± 0.02			

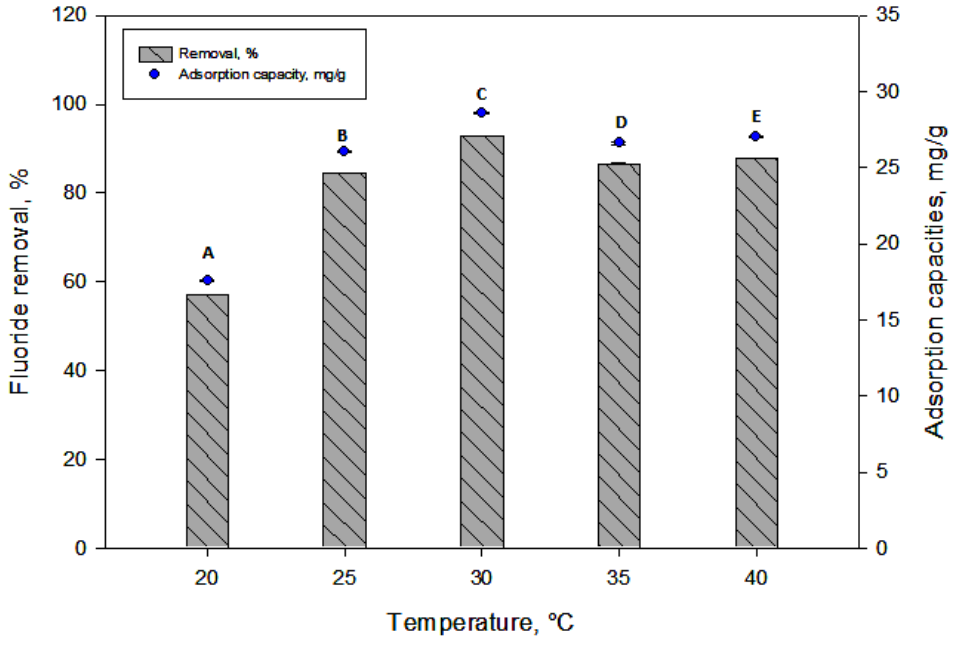

Fig. 8. Effect of temperature on fluoride removal percentage (%) and adsorption capacity (Q_e) using; 30 mg/L initial fluoride concentration, 1 g/L of Ce-Ti-Fe oxide nanomaterials and shaking at 200 rpm for 60 min. Statistical data analysis using ANOVA was illustrated by letters A, B, C, D, and E.

3.6. Application of Ce-Ti@Fe_3O_4 nano adsorbent for fluoride removal from real water sample

The efficiency of the magnetic Ce-Ti@Fe_3O_4 NPs for fluoride removal from drinking water sample spiked with 10 mg/L of fluoride was studied. The results (Table 5) proved that the Ce-Ti@Fe_3O_4 adsorbent had a strong affinity for fluoride removal in the presence of other anions. The removal percentage of fluoride decreased from about 99 to 73 % (0.11 to 2.94 mg/L) at ambient temperature due to the presence of other co-existing anions. In addition, the adsorbent posed affinity towards other anions, under the tested conditions, with removal percentage of 15, 36, 11, and 99 % for chloride (Cl^-), nitrite (NO_2^-), sulphate (SO_4^{2-}), and nitrate (NO_3^-) respectively. This could be attributed to some anions competition and others enhanced columbic repulsion forces with fluoride for the active sites (Onyango et al., 2004). Moreover, increasing the temperature from 25 to 30 °C increased the removal percentage of fluoride from 73 to 87 % (2.94 to 1.44 mg/L) being the residual concentration of fluoride 1.44 mg/L, which is below the maximum acceptable level, 1.50 mg/L. Furthermore, the removal percentage increased to be 18 and 100 % for the chloride and nitrate anions, respectively while it decreased to be 35 and 10 % for the nitrite and sulphate anions, respectively. Subsequently, the novel magnetic Ce-Ti@Fe_3O_4 nanomaterial is a promising and efficient material for anions removal from water not only fluoride, but also for nitrate, nitrite, chloride, and sulphate.

468 **Table 5.** Efficiency of the Ce-Ti@Fe_3O_4 adsorbents on the fluoride removal from drinking
469 water

Anions	Anions concentration, mg/L		
	Spiked tap water	After adsorption[a]	After adsorption[b]
Fluoride	10.93 ± 0.13 (< 0.010[c])	2.94 ± 0.23	1.44 ± 0.04
Chloride	32.71 ± 0.05	27.86 ± 0.02	26.78 ± 0.04
Nitrite as NO_2^-	1.51 ± 0.01	0.97 ± 0.02	0.98 ± 0.03
Sulphate	16.14 ± 0.02	14.33 ± 0.10	14.47 ± 0.04
Nitrate as NO_3^-	3.16 ± 0.01	0.01 ± 0.00	N.D[d]

a: Adsorption at 25 °C, 1.0 g/L Ce-Ti-Fe oxide, 60 min adsorption time, and 200 rpm.
b: Adsorption at 30 °C, 1.0 g/L Ce-Ti-Fe oxide, 60 min adsorption time, and 200 rpm.
c: Fluoride concentration in drinking water before spiking.
d: N.D: Not detected

470

471 **4. Conclusions**

472 The synthesized magnetic core-shell Ce-Ti@Fe_3O_4 NPs showed high efficiency for
473 fluoride removal and high sorption capacity. The maximum adsorption capacity was 91.04
474 mg/g at pH 7, which outperformed many reported adsorbents and the synthesized Ce-Ti
475 oxides NPs (44.37mg/L). Ce-Ti@Fe_3O_4 nanomaterial as adsorbent is applicable over a
476 wide pH range (from 5 to 11) and shows a fast adsorption rate. Moreover, it is easy to
477 recover from the reaction mixture for further reuse and it has been used for 5 cycles. The
478 reusability of the NPs under those conditions was evaluated, showing a little modification
479 in its structure after the cycles and no Ce release is presented in the treated water. In
480 addition to the spontaneous adsorption process, it was shown an increasing of the
481 adsorption capacities by increasing the temperature. Furthermore, the physical sorption
482 mechanism was estimated according to the Dubbinin-Radushkevich isotherm model: anion
483 exchange between the hydroxyl group on the surface of the adsorbents and fluoride ions

484 was involved. Besides, the efficacy of the Ce-Ti@Fe_3O_4 NPs as adsorbent was
485 demonstrated for a real water matrix by spiking 10 mg/L of fluoride in drinking water, as it
486 showed a residual fluoride concentration of 1.44 mg/L. Therefore, magnetic Ce-Ti@Fe_3O_4
487 nanomaterial was arbitrated to be a suitable adsorbent to treat fluoride contaminated water
488 to achieve the quality standard of drinking water.
489
490 **Acknowledgement**
491 The author, Ahmad Abo Markeb, appreciated and would like to thank the Ministry of
492 Higher Education of Egypt for the Ph.D. external mission grant.
493
494 **Appendix A. Supplementary information**
495 Supplementary data associated with this article can be found in the online version.
496
497 **References**
498 Abo Markeb A, Ordosgoitia L, Alonso A, Sanchez A, Font X. Novel magnetic core-shell Ce-
499 Ti@Fe_3O_4 nanoparticles as adsorbent for water contaminants removal. RSC Adv.
500 2016.
501 Amor Z, Bariou B, Mameri N, Taky M, Nicolas S, Elmidaoui A. Fluoride removal from
502 brackish water by electrodialysis. Desalination 2001; 133: 215-223.
503 Babaeivelni K, Khodadoust AP. Adsorption of fluoride onto crystalline titanium dioxide:
504 Effect of pH, ionic strength, and co-existing ions. J. Colloid Interf. Sci. 2013; 394:
505 419-427.

506 Bhatnagar A, Kumar E, Sillanpää M. Fluoride removal from water by adsorption—A review.
507 Chem. Eng. J. 2011; 171: 811-840.
508 Biswas K, Bandhoyapadhyay D, Ghosh UC. Adsorption kinetics of fluoride on iron(III)-
509 zirconium(IV) hybrid oxide. Adsorption 2007; 13: 83-94.
510 Biswas K, Debnath S, Ghosh UC. Physicochemical Aspects on Fluoride Adsorption for
511 Removal from Water by Synthetic Hydrous Iron(III) – Chromium(III) Mixed Oxide.
512 Sep. Sci. Technol. 2010; 45: 472-485.
513 Biswas K, Gupta K, Ghosh UC. Adsorption of fluoride by hydrous iron(III)–tin(IV) bimetal
514 mixed oxide from the aqueous solutions. Chem. Eng. J. 2009; 149: 196-206.
515 Chai L, Wang Y, Zhao N, Yang W, You X. Sulfate-doped Fe_3O_4/Al_2O_3 nanoparticles as a
516 novel adsorbent for fluoride removal from drinking water. Water Res. 2013; 47: 4040-
517 4049.
518 Chang MF, Liu JC. Precipitation removal of fluoride from semiconductor wastewater. J.
519 Environ. Eng. 2007; 133: 419-425.
520 Chen L, He B-Y, He S, Wang T-J, Su C-L, Jin Y. Fe—Ti oxide nano-adsorbent synthesized
521 by co-precipitation for fluoride removal from drinking water and its adsorption
522 mechanism. Powder Technol. 2012; 227: 3-8.
523 Chen L, Wang T-J, Wu H-X, Jin Y, Zhang Y, Dou X-M. Optimization of a Fe–Al–Ce nano-
524 adsorbent granulation process that used spray coating in a fluidized bed for fluoride
525 removal from drinking water. Powder Technol. 2011; 206: 291-296.
526 Tso CP, Zhung CM, Shih YH, Tseng YM, Wu SC, Doong RA. Stability of metal oxide
527 nanoparticles in aqueous solutions. Water Sci. Technol. 2010; 61: 127-33.

528 Dai S, Ren D, Ma S. The cause of endemic fluorosis in western Guizhou Province, Southwest
529 China. Fuel 2004; 83: 2095-2098.
530 Deng S, Liu H, Zhou W, Huang J, Yu G. Mn–Ce oxide as a high-capacity adsorbent for
531 fluoride removal from water. J. Hazard. Mater. 2011; 186: 1360-1366.
532 Deniz F. Adsorption Properties of Low-Cost Biomaterial Derived from Prunus amygdalus L.
533 for Dye Removal from Water. Scientific World J. 2013; 2013: 961671.
534 Dorado AD, Lafuente J, Gabriel D, Gamisans X. The role of water in the performance of
535 biofilters: Parameterization of pressure drop and sorption capacities for common
536 packing materials. J. Hazard. Mater. 2010; 180: 693-702.
537 Drinking-water pi. Background document for development of WHO Guidelines for Drinking-
538 water Quality. WHO 2004.
539 Giammar DE, Maus CJ, Xie L. Effects of Particle Size and Crystalline Phase on Lead
540 Adsorption to Titanium Dioxide Nanoparticles. Environ.l Eng. Sci. 2006; 24: 85-95.
541 Gupta P, Kumar A. Fluoride levels of bottled and tap water sources in Agra City, India.
542 Fluoride 2012; 45: 307-310.
543 Habuda-Stanić M, Ravančić M, Flanagan A. A Review on Adsorption of Fluoride from
544 Aqueous Solution. Materials 2014; 7: 6317.
545 Ishihara T, Shuto Y, Ueshima S, Ngee HL, Nishiguchi H, Takita Y. Titanium Hydroxide as a
546 New Inorganic Fluoride Ion Exchanger. J. Ceram. Soc. Jpn 2002; 110: 801-803.
547 Karthikeyan M, Kumar KKS, Elango KP. Batch sorption studies on the removal of fluoride
548 ions from water using eco-friendly conducting polymer/bio-polymer composites.
549 Desalination 2011; 267: 49-56.

550 Kumar E, Bhatnagar A, Kumar U, Sillanpää M. Defluoridation from aqueous solutions by
551 nano-alumina: Characterization and sorption studies. J. Hazard. Mater. 2011; 186:
552 1042-1049.
553 Lee G, Chen C, Yang S-T, Ahn W-S. Enhanced adsorptive removal of fluoride using
554 mesoporous alumina. Micropor. Mesopor. Mater. 2010; 127: 152-156.
555 Li Z, Deng S, Zhang X, Zhou W, Huang J, Yu G. Removal of fluoride from water using
556 titanium-based adsorbents. Front. Environ. Sci. Eng. China 2010; 4: 414-420.
557 Liu H, Deng S, Li Z, Yu G, Huang J. Preparation of Al–Ce hybrid adsorbent and its
558 application for defluoridation of drinking water. J. Hazard. Mater. 2010; 179: 424-430.
559 Liu R, Gong W, Lan H, Gao Y, Liu H, Qu J. Defluoridation by freshly prepared aluminum
560 hydroxides. Chem. Eng. J. 2011; 175: 144-149.
561 Mahramanlioglu M, Kizilcikli I, Bicer IO. Adsorption of fluoride from aqueous solution by
562 acid treated spent bleaching earth. J. Fluor. Chem. 2002; 115: 41-47.
563 Martínez-Acuña MI, Mercado-Reyes M, Alegría-Torres JA, Mejía-Saavedra JJ. Preliminary
564 human health risk assessment of arsenic and fluoride in tap water from Zacatecas,
565 México. Environ. Monit. Assess. 2016; 188: 476.
566 Martos M, Julián-López B, Folgado JV, Cordoncillo E, Escribano P. Sol–Gel Synthesis of
567 Tunable Cerium Titanate Materials. Eur. J. Inorg. Chem. 2008; 2008: 3163-3171.
568 Meenakshi, Maheshwari RC. Fluoride in drinking water and its removal. J. Hazard. Mater.
569 2006; 137: 456-463.
570 Meenakshi S, Viswanathan N. Identification of selective ion-exchange resin for fluoride
571 sorption. J. Colloid Interf. Sci. 2007; 308: 438-450.

572 Minju N, Venkat Swaroop K, Haribabu K, Sivasubramanian V, Senthil Kumar P. Removal of
573 fluoride from aqueous media by magnesium oxide-coated nanoparticles. Desalin.
574 Water Treat. 2013; 53: 2905-2914.
575 Mohan D, Kumar S, Srivastava A. Fluoride removal from ground water using magnetic and
576 nonmagnetic corn stover biochars. Ecol. Eng. 2014; 73: 798-808.
577 Mohapatra M, Anand S, Mishra BK, Giles DE, Singh P. Review of fluoride removal from
578 drinking water. J. Environ. Manage. 2009; 91: 67-77.
579 N. Gandhi, D. Sirisha, S. Asthana, A. Manjusha. Adsorption studies of fluoride on multani
580 matti and red soil. Res. J. Chem. Sci. 2012; 2: 32-37.
581 Onyango MS, Kojima Y, Aoyi O, Bernardo EC, Matsuda H. Adsorption equilibrium
582 modeling and solution chemistry dependence of fluoride removal from water by
583 trivalent-cation-exchanged zeolite F-9. J. Colloid Interf. Sci. 2004; 279: 341-350.
584 Pattanaik M, Bhaumik SK. Adsorption behaviour of polyvinyl pyrrolidone on oxide surfaces.
585 Mater. Lett. 2000; 44: 352-360.
586 Petersen PE, Bourgeois D, Ogawa H, Estupinan-Day S, Ndiaye C. The global burden of oral
587 diseases and risks to oral health. Bull. World Health Organ. 2005; 83: 661-669.
588 Qu X, Alvarez PJJ, Li Q. Applications of nanotechnology in water and wastewater treatment.
589 Water Res. 2013; 47: 3931-3946.
590 Rafique A, Awan MA, Wasti A, Qazi IA, Arshad M. Removal of Fluoride from Drinking
591 Water Using Modified Immobilized Activated Alumina. Journal of Chemistry 2013;
592 2013: 7.
593 Raichur AM, Jyoti Basu M. Adsorption of fluoride onto mixed rare earth oxides. Sep. Purif.
594 Technol. 2001; 24: 121-127.

595 Riahi F, Bagherzadeh M, Hadizadeh Z. Modification of Fe_3O_4 superparamagnetic
596 nanoparticles with zirconium oxide; preparation, characterization and its application
597 toward fluoride removal. RSC Adv. 2015; 5: 72058-72068.
598 Sehn P. Fluoride removal with extra low energy reverse osmosis membranes: three years of
599 large scale field experience in Finland. Desalination 2008; 223: 73-84.
600 Shen F, Chen X, Gao P, Chen G. Electrochemical removal of fluoride ions from industrial
601 wastewater. Chem. Eng. Sci. 2003; 58: 987-993.
602 Shiklomanov IA. Appraisal and assessment of world water resources. Water Int. 2000; 25: 11-
603 32.
604 Singh K, Lataye DH, Wasewar KL, Yoo CK. Removal of fluoride from aqueous solution:
605 Status and techniques. Desalin. and Water Treat. 2013; 51: 3233-3247.
606 Sinha S, Pandey K, Mohan D, Singh KP. Removal of Fluoride from Aqueous Solutions by
607 Eichhornia crassipes Biomass and Its Carbonized Form. Ind. Eng. Chem. Res. 2003;
608 42: 6911-6918.
609 Sivasankar V, Ramachandramoorthy T, Darchen A. Manganese dioxide improves the
610 efficiency of earthenware in fluoride removal from drinking water. Desalination 2011;
611 272: 179-186.
612 Solangi IB, Memon S, Bhanger MI. Removal of fluoride from aqueous environment by
613 modified Amberlite resin. J. Hazard. Mater. 2009; 171: 815-819.
614 Sujana MG, Anand S. Iron and aluminium based mixed hydroxides: A novel sorbent for
615 fluoride removal from aqueous solutions. Appl. Surf. Sci. 2010; 256: 6956-6962.
616 Tang D, Zhang G. Efficient removal of fluoride by hierarchical Ce–Fe bimetal oxides
617 adsorbent: Thermodynamics, kinetics and mechanism. Chem. Eng. J. 2016; 283: 721-
618 729.

Taylor NS, Merrifield R, Williams TD, Chipman JK, Lead JR, Viant MR. Molecular toxicity of cerium oxide nanoparticles to the freshwater alga Chlamydomonas reinhardtii is associated with supra-environmental exposure concentrations. Nanotoxicology 2016; 10: 32-41.

Teng S-X, Wang S-G, Gong W-X, Liu X-W, Gao B-Y. Removal of fluoride by hydrous manganese oxide-coated alumina: Performance and mechanism. J. Hazard. Mater. 2009; 168: 1004-1011.

Teutli-Sequeira A, Solache-Ríos M, Martínez-Miranda V, Linares-Hernández I. Behavior of Fluoride Removal by Aluminum Modified Zeolitic Tuff and Hematite in Column Systems and the Thermodynamic Parameters of the Process. Water Air Soil Pollut. 2015; 226: 1-15.

Tomar V, Prasad S, Kumar D. Adsorptive removal of fluoride from water samples using Zr–Mn composite material. Microchemical J. 2013; 111: 116-124.

Velizarov S, Crespo JG, Reis MA. Removal of inorganic anions from drinking water supplies by membrane bio/processes. Reviews in Environmental Science and Biotechnology 2004; 3: 361-380.

Vinati A, Mahanty B, Behera SK. Clay and clay minerals for fluoride removal from water: A state-of-the-art review. Appl. Clay Sci. 2015; 114: 340-348.

Viswanathan G, Jaswanth A, Gopalakrishnan S, Siva ilango S. Mapping of fluoride endemic areas and assessment of fluoride exposure. Sci. Total Environ. 2009; 407: 1579-1587.

Wang B, Wei Q, Qu S. Synthesis and Characterization of Uniform and Crystalline Magnetite Nanoparticles via Oxidation-precipitation and Modified co-precipitation Methods. Int. J. Electrochem. Sci. 2013; 8: 3786 -3793.

642 WHO. Chemical fact sheets: fluoride. In: Guidelines for drinking-water quality (electronic
643 resource): incorporation first addendum. 2006; 1 third edition, Geneva: 375-377.
644 Y. Xiuru, S. Kuanxiu, W. Jianping a, Zhaohui Y. Preparation of CeO_2-TiO_2/SiO_2 and its
645 removal properties for fluoride ion. J. Rare Earths 1998; 16: 279-280.
646 Zhang C, Chen L, Wang T-J, Su C-L, Jin Y. Synthesis and properties of a magnetic core–shell
647 composite nano-adsorbent for fluoride removal from drinking water. Appl. Surf. Sci.
648 2014; 317: 552-559.
649 Zhang C, Li Y, Wang T-J, Jiang Y, Wang H. Adsorption of drinking water fluoride on a
650 micron-sized magnetic Fe_3O_4@Fe-Ti composite adsorbent. Appl. Surf. Sci. 2016; 363:
651 507-515.
652 Zhang K, Wu S, Wang X, He J, Sun B, Jia Y, et al. Wide pH range for fluoride removal from
653 water by MHS-MgO/$MgCO_3$ adsorbent: Kinetic, thermodynamic and mechanism
654 studies. J. Colloid Interf. Sci. 2015; 446: 194-202.
655 Zhang Y, Yang M, Dou XM, He H, Wang DS. Arsenate adsorption on an Fe-Ce bimetal oxide
656 adsorbent: Role of surface properties. Environ. Sci. Technol. 2005; 39: 7246-7253.
657 Zhao X, Wang J, Wu F, Wang T, Cai Y, Shi Y, et al. Removal of fluoride from aqueous
658 media by Fe_3O_4@$Al(OH)_3$ magnetic nanoparticles. J. Hazard. Mater. 2010; 173: 102-
659 109.

660
661
662